SPECTRAL UNMIXING OF HYPERSPECTRAL IMAGES USING A HIERARCHICAL BAYESIAN MODEL

Nicolas Dobigeon and Jean-Yves Tourneret

IRIT/ENSEEIHT/TéSA, 2 rue Charles Camichel, BP 7122, 31071 Toulouse cedex 7, France

Nicolas.Dobigeon@enseeiht.fr, Jean-Yves.Tourneret@enseeiht.fr

ABSTRACT

This paper addresses the problem of hyperspectral image unmixing. A new hierarchical Bayesian algorithm is proposed to estimate the coefficients of a linear mixture of spectra associated to a given pixel of the image. Appropriate priors are introduced to guaranty the positivity and additivity constraints inherent to the mixture coefficients. These coefficients referred to as abundances are then estimated from their posterior following the principles of Bayesian inference. The estimation is performed by using a Gibbs sampling strategy which generates samples distributed according the abundance posterior distribution. These samples are then averaged yielding the abundance minimum mean square error estimator.

Index Terms— Bayesian inference, Monte Carlo methods, spectral unmixing, hyperspectral images.

1. INTRODUCTION

Observing a given scene in different wavelength intervals is a classical way of obtaining high quality images. These images include multispectral and hyperspectral images. The pixels of hyperspectral images result from the mixture of different pure materials called endmembers. Hyperspectral sensors provide a spectrum for each pixel of the image. The unmixing problem consist of decomposing the spectrum associated to a given pixel as a mixture of spectra associated to different endmembers and to estimate the coefficients of this mixture usually referred to as abundances. The unmixing problem has received much attention in the literature (see for instance [1] for a recent review on this problem and references therein) and is classically divided into three steps 1) dimension reduction, 2) endmember determination and 3) inversion. This paper concentrates on the inversion step which is fundamental in any unmixing algorithm.

The difficulty of the inversion problem is mainly due to the additivity and positivity constraints that the abundances have to satisfy. A lot of inversion methods which have been studied in the literature have been formulated as constrained least squares problems [2, 3]. The idea of these methods is to estimate the abundances by minimizing the usual least-squares error, by constraining the solutions to satisfy appropriate additivity and positivity constraints. This paper proposes a new approach which defines prior distributions for the abundances which satisfy the positivity and additivity constraints. This results in a hierarchical Bayesian algorithm for unmixing hyperspectral images. The proposed algorithm allows us to derive the *a posteriori* distribution of the abundances, which can be used to estimate these parameters by means of the minimum mean square error (MMSE) or maximum *a posteriori* (MAP) estimators. However, the posterior distribution of the abundances is also interesting to derive confidence intervals or theoretical variances for these parameters.

The paper is organized as follows. The linear mixing model used for hyperspectral images is presented in Section 2. Section 3 describes the different elements of the hierarchical model used to address the unmixing problem. Section 4 studies a Gibbs sampler which allows one to generate samples distributed according to the abundance posterior distribution. Some simulation results on synthetic and real data are presented in Sections 5 and 6. Conclusions are reported in Section 7.

2. LINEAR MIXING MODEL

This section defines the classical analytical model which will be used to perform spectral unmixing. Non-linear mixing has already received some attention in the literature. However, there are several obstacles for implementing nonlinear models (the reader is invited to consult [1] for more details). This paper concentrates on the most commonly used linear unmixing problem which constitutes a good approximation in the reflective domain ranging from $0.4\mu m$ to $2.5\mu m$ (see [1, 4] or more recently [5]). The linear mixing model (LMM) assumes that the L-spectrum $\mathbf{y} = [y_1, \ldots, y_L]^{\mathsf{T}}$ of a mixed pixel is a linear combination of R spectra $\mathbf{m}_r$ contaminated by additive white noise:

$$\mathbf{y} = \sum_{r=1}^{R} \mathbf{m}_r \alpha_r + \mathbf{n}, \tag{1}$$

where $\mathbf{m}_r = [m_{r,1}, \ldots, m_{r,L}]^{\mathsf{T}}$ denotes the spectrum of the r^{th} material, α_r is the fraction of the r^{th} material in the pixel (or r^{th} *abundance*), R is the number of pure materials (or *endmembers*) present in all the observed scene, L is the number of available spectral bands for the image and $\mathbf{n} = [n_1, \ldots, n_L]^{\mathsf{T}}$ is the additive white noise sequence. The noise sequence is classically assumed to be an independent and identically distributed (i.i.d.) zero-mean Gaussian sequence with variance σ^2, denoted as $\mathbf{n} \sim \mathcal{N}(\mathbf{0}_L, \sigma^2 \mathbf{I}_L)$, where $\mathbf{I}_L$ is the identity matrix of dimension $L \times L$. Due to physical considerations, the fraction vector $\boldsymbol{\alpha}^+ = [\alpha_1, \ldots, \alpha_R]^{\mathsf{T}}$ satisfies the following positivity and additivity constraints:

$$\begin{cases} \alpha_r \geq 0, \ \forall r = 1, \ldots, R, \\ \sum_{r=1}^{R} \alpha_r = 1. \end{cases} \tag{2}$$

The R endmembers spectra $\mathbf{m}_r$ are assumed to be known in this paper. As a consequence, the proposed methodology has to be coupled with one of the many identification techniques to estimate endmember spectra. These techniques include geometrical methods [6, 7] or statistical procedures [8, 9].

3. HIERARCHICAL BAYESIAN MODEL

This section introduces a hierarchical Bayesian model to estimate the unknown parameter vector $\boldsymbol{\alpha}$ under the constraints specified in Eq. (2). This model is based on the likelihood of the observations and on prior distributions for the unknown parameters.

3.1. Likelihood

The LMM defined in Eq. (1) and the statistical properties of the noise vector $\mathbf{n}$ yield $\mathbf{y} \sim \mathcal{N}(\mathbf{M}^+\boldsymbol{\alpha}^+, \sigma^2\mathbf{I}_L)$, where $\mathbf{M}^+ = [\mathbf{m}_1, \ldots, \mathbf{m}_R]$ and $\boldsymbol{\alpha}^+ = [\alpha_1, \ldots, \alpha_R]^\mathsf{T}$. Consequently, the likelihood function of $\mathbf{y}$ can be expressed as:

$$f(\mathbf{y}|\boldsymbol{\alpha}^+, \sigma^2) = \left(\frac{1}{2\pi\sigma^2}\right)^{\frac{L}{2}} \exp\left[-\frac{\left\|\mathbf{y} - \mathbf{M}^+\boldsymbol{\alpha}^+\right\|^2}{2\sigma^2}\right], \quad (3)$$

where $\|\mathbf{x}\|^2 = \mathbf{x}^\mathsf{T}\mathbf{x}$ is the standard L^2 norm.

3.2. Parameter priors

The abundance vector can be decomposed as $\boldsymbol{\alpha}^+ = [\boldsymbol{\alpha}^\mathsf{T}, \alpha_R]^\mathsf{T}$, where $\boldsymbol{\alpha} = [\alpha_1, \ldots, \alpha_{R-1}]^\mathsf{T}$ and $\alpha_R = 1 - \sum_{r=1}^{R-1}\alpha_r$. A truncated multivariate normal distribution is chosen as prior distribution for $\boldsymbol{\alpha}$:

$$\boldsymbol{\alpha} \sim \mathcal{N}_\mathbb{S}(\mathbf{0}_{R-1}, \sigma_0^2\mathbf{I}_{R-1}), \quad (4)$$

where

$$\mathbb{S} = \left\{\boldsymbol{\alpha} \,\middle|\, \alpha_r \geq 0,\ \forall r = 1, \ldots, R-1,\ \sum_{r=1}^{R-1}\alpha_r \leq 1\right\}, \quad (5)$$

$\mathcal{N}_\mathbb{S}(\boldsymbol{\theta}, \boldsymbol{\Sigma})$ denotes the multivariate normal distribution with mean vector $\boldsymbol{\theta}$ and covariance matrix $\boldsymbol{\Sigma}$ truncated to the domain $\mathbb{S}$, and $\mathbf{0}_{R-1}$ is the vector made of $R-1$ zeros. The probability density function (pdf) of this truncated multivariate normal distribution denoted as $\phi_\mathbb{S}(\cdot|\boldsymbol{\theta}, \boldsymbol{\Sigma})$ satisfies the following relation:

$$\phi_\mathbb{S}(\mathbf{x}|\boldsymbol{\theta}, \boldsymbol{\Sigma}) \propto \phi(\mathbf{x}|\boldsymbol{\theta}, \boldsymbol{\Sigma})\mathbf{1}_\mathbb{S}(\mathbf{x}), \quad (6)$$

where $\phi(\cdot|\boldsymbol{\theta}, \boldsymbol{\Sigma})$ is the standard Gaussian pdf with mean vector $\boldsymbol{\theta}$ and covariance matrix $\boldsymbol{\Sigma}$, $\mathbf{1}_\mathbb{S}(\mathbf{.})$ is the indicator function defined on $\mathbb{S}$ and the symbol $\propto$ means "proportional to". Note that the pdf $\phi_\mathbb{S}$ is parametrized by the adjustable hyperparameter σ_0^2.
A non-informative conjugate prior is chosen for σ^2:

$$\sigma^2 \sim \mathcal{IG}\left(\frac{\nu}{2}, \frac{\gamma}{2}\right), \quad (7)$$

where $\mathcal{IG}\left(\frac{\nu}{2}, \frac{\gamma}{2}\right)$ denotes the inverse-gamma distribution with parameters $\frac{\nu}{2}$ and $\frac{\gamma}{2}$. The hyperparameter ν will be fixed to $\nu = 2$ (as in [10]) whereas γ is an adjustable hyperparameter.

3.3. Hyperparameter priors

The hyperparameter vector associated to the parameter priors defined above is $\boldsymbol{\Phi} = \left\{\gamma, \sigma_0^2\right\}$. Of course, the quality of the unmixing procedure depends on the values of these hyperparameters. The hierarchical bayesian approach developed in this paper requires to define hyperparameter priors that are detailed in this section. The priors for γ and σ_0^2 are a non-informative Jeffrey's prior and a conjugate inverse-gamma distribution respectively:

$$f(\gamma) = \frac{1}{\gamma}\mathbf{1}_{\mathbb{R}^+}(\gamma), \qquad \sigma_0^2 \sim \mathcal{IG}\left(\frac{\rho}{2}, \frac{\psi}{2}\right). \quad (8)$$

The values of parameters ρ and ψ will be adjusted in order to provide a "vague" prior, reflecting the lack of knowledge regarding σ_0^2. Assuming the independence between the individual hyperparameters, the full hyperparameter prior distribution $\boldsymbol{\Phi}$ can be written:

$$f(\boldsymbol{\Phi}) \propto \frac{1}{\gamma}\left(\frac{1}{\sigma_0^2}\right)^{\frac{\rho}{2}+1} \exp\left[-\frac{\psi}{2\sigma_0^2}\right]\mathbf{1}_{\mathbb{R}^+}(\gamma). \quad (9)$$

3.4. Posterior distribution of $\boldsymbol{\theta}$

The posterior distribution of the unknown parameter vector $\boldsymbol{\theta} = \left\{\boldsymbol{\alpha}, \sigma^2\right\}$ can be computed from the following hierarchical structure:

$$f(\boldsymbol{\theta}|\mathbf{y}) = \int f(\boldsymbol{\theta}, \boldsymbol{\Phi}|\mathbf{y})d\boldsymbol{\Phi} \propto \int f(\mathbf{y}|\boldsymbol{\theta})f(\boldsymbol{\theta}|\boldsymbol{\Phi})f(\boldsymbol{\Phi})d\boldsymbol{\Phi}, \quad (10)$$

where $f(\mathbf{y}, \boldsymbol{\theta})$ and $f(\boldsymbol{\Phi})$ are defined in Eq.'s (3) and (9) respectively. Moreover, by assuming the independence between σ^2 and $\boldsymbol{\alpha}$, the following result can be obtained:

$$f(\boldsymbol{\theta}|\boldsymbol{\Phi}) = f(\boldsymbol{\alpha}|\sigma_0^2)f(\sigma^2|\nu, \gamma). \quad (11)$$

This hierarchical structure allows one to integrate out the hyperparameter γ. In addition, by using the approximation [11]:

$$K_\mathbb{S}\left(\sigma_0^2\right) \triangleq \int_\mathbb{S} \exp\left[-\frac{\|\boldsymbol{\alpha}\|^2}{2\sigma_0^2}\right]d\boldsymbol{\alpha} \approx \frac{1}{(R-1)!}, \quad (12)$$

the hyperparameter σ_0^2 can also be integrated out from the joint distribution $f(\boldsymbol{\theta}, \boldsymbol{\Phi}|\mathbf{y})$, yielding the approximated posterior:

$$f\left(\boldsymbol{\alpha}, \sigma^2|\mathbf{y}\right) \propto \left(\frac{1}{\sigma^2}\right)^{\frac{L}{2}+1} \exp\left[-\frac{\left\|\mathbf{y} - \mathbf{M}^+\boldsymbol{\alpha}^+\right\|^2}{2\sigma^2}\right] \times \left[\psi + \|\boldsymbol{\alpha}\|^2\right]^{-\frac{\rho}{2}} \mathbf{1}_\mathbb{S}(\boldsymbol{\alpha}). \quad (13)$$

The next section shows that an appropriate Gibbs sampling strategy allows one to generate samples distributed according to the joint distribution $f(\boldsymbol{\alpha}, \sigma^2|\mathbf{y})$.

4. A GIBBS SAMPLER FOR ABUNDANCE ESTIMATION

Sampling according to $f(\boldsymbol{\alpha}, \sigma^2|\mathbf{y})$ can be achieved by a Gibbs sampler whose steps are detailed in Subsections 4.1 and 4.2.

4.1. Generation of samples distributed according to $f(\boldsymbol{\alpha}|\sigma^2, \mathbf{y})$

To sample according to $f(\boldsymbol{\alpha}|\sigma^2, \mathbf{y})$, it is very convenient to generate samples distributed according to $f(\boldsymbol{\alpha}, \sigma_0^2|\sigma^2, \mathbf{y})$ by using the following procedures.
• **Generation of samples according to** $f(\sigma_0^2|\boldsymbol{\alpha}, \sigma^2, \mathbf{y})$: The posterior distribution of σ_0^2 conditioned upon $\left(\boldsymbol{\alpha}, \sigma^2, \mathbf{y}\right)$ expresses as:

$$f\left(\sigma_0^2|\boldsymbol{\alpha}, \sigma^2\mathbf{y}\right) \propto \frac{1}{K_\mathbb{S}\left(\sigma_0^2\right)}\left(\frac{1}{\sigma_0^2}\right)^{\frac{\rho}{2}+1} \exp\left[-\frac{\psi + \|\boldsymbol{\alpha}\|^2}{2\sigma_0^2}\right].$$

Using the approximation in Eq. (12), the following result is obtained:

$$\sigma_0^2|\boldsymbol{\alpha}, \sigma^2, \mathbf{y} \sim \mathcal{IG}\left(\frac{\rho}{2}, \frac{\psi + \|\boldsymbol{\alpha}\|^2}{2}\right). \quad (14)$$

• **Generation of samples according to** $f(\boldsymbol{\alpha}|\sigma_0^2, \sigma^2, \mathbf{y})$: By denoting $\mathbf{M} = [\mathbf{m}_1, \ldots \mathbf{m}_{R-1}]$, straightforward computations yield:

$$f\left(\boldsymbol{\alpha}|\sigma_0^2, \sigma^2, \mathbf{y}\right) \propto \exp\left[-\frac{(\boldsymbol{\alpha} - \boldsymbol{\mu})^\mathsf{T}\boldsymbol{\Lambda}^{-1}(\boldsymbol{\alpha} - \boldsymbol{\mu})}{2}\right]\mathbf{1}_\mathbb{S}(\boldsymbol{\alpha}), \quad (15)$$

where

$$\begin{cases} \boldsymbol{\Lambda} = \left[\frac{1}{\sigma^2}\left(\mathbf{M} - \mathbf{m}_R\mathbf{u}^\mathsf{T}\right)^\mathsf{T}\left(\mathbf{M} - \mathbf{m}_R\mathbf{u}^\mathsf{T}\right) + \frac{1}{\sigma_0^2}\mathbf{I}_{R-1}\right]^{-1}, \\ \boldsymbol{\mu} = \boldsymbol{\Lambda}\left[\frac{1}{\sigma^2}\left(\mathbf{M} - \mathbf{m}_R\mathbf{u}^\mathsf{T}\right)^\mathsf{T}(\mathbf{y} - \mathbf{m}_R)\right], \end{cases} \quad (16)$$

with $\mathbf{u} = [1, \ldots, 1]^\mathsf{T} \in \mathbb{R}^{R-1}$. As a consequence, $\boldsymbol{\alpha}|\sigma_0^2, \sigma^2, \mathbf{y}$ is distributed according to a truncated Gaussian distribution:

$$\boldsymbol{\alpha}|\sigma_0^2, \sigma^2, \mathbf{y} \sim \mathcal{N}_\mathbb{S}\left(\boldsymbol{\mu}, \boldsymbol{\Lambda}\right). \quad (17)$$

The generation of $\boldsymbol{\alpha}|\sigma_0^2, \sigma^2, \mathbf{y}$ is achieved using a standard accept-reject procedure.

4.2. Generation of samples distributed according to $f(\sigma^2|\alpha, \mathbf{y})$

Looking carefully at the joint distribution $f(\sigma^2, \boldsymbol{\alpha}|\mathbf{y})$, the conditional distribution of $\sigma^2|\boldsymbol{\alpha}, \mathbf{y}$ is the following inverse gamma distribution:

$$\sigma^2|\boldsymbol{\alpha}, \mathbf{y} \sim \mathcal{IG}\left(\frac{L}{2}, \frac{\left\|\mathbf{y} - \mathbf{M}^+\boldsymbol{\alpha}^+\right\|^2}{2}\right). \quad (18)$$

5. SIMULATION RESULTS ON SYNTHETIC DATA

The accuracy of the proposed abundance estimation procedure is first illustrated by unmixing a synthetic pixel resulting from the combination of three pure components. These components have been extracted from the spectral libraries that are distributed with the ENVI software [12, p.1035] and are representative of a urban or suburban environment: construction concrete, green grass and dark yellowish brown micaceous loam. The proportions of these components are $\alpha_1 = 0.3$, $\alpha_2 = 0.6$ and $\alpha_3 = 0.1$, respectively. The observations have been corrupted by an additive Gaussian noise with variance $\sigma^2 = 0.025$ (the corresponding signal to noise ratio is about SNR $= 15$dB). The endmember spectra and the resulting spectrum of the mixed pixel are plotted in Fig. 1.

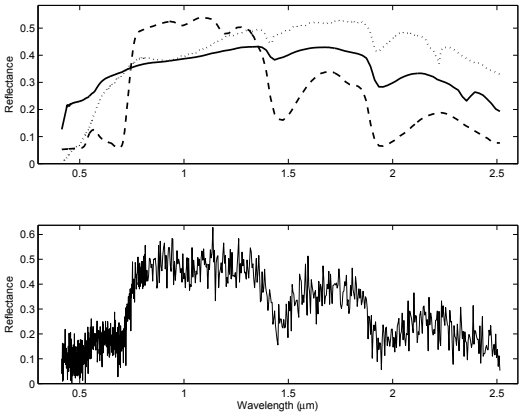

Fig. 1. Top: endmember spectra: construction concrete (solid line), green grass (dashed line), dark yellowish brown micaceous loam (dotted line). Bottom: resulting spectrum of the mixed pixel.

The values of parameters ρ and ψ have been chosen as $\rho = 4$ and $\psi = 100$, yielding a vague prior for σ_0^2. Fig. 2 shows the marginal posterior distributions of the abundance coefficients α_r $(r = 1, 2, 3)$ obtained for $N_{\mathrm{MC}} = 20000$ iterations (including $N_{\mathrm{bi}} = 100$ burn-in iterations). These distributions are in good agreement with the actual values of $\boldsymbol{\alpha}^+ = [0.3, 0.6, 0.1]^{\mathsf{T}}$.

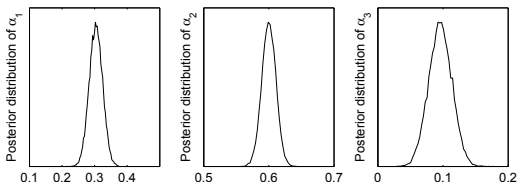

Fig. 2. Posterior distributions of the estimated abundances $[\alpha_1, \alpha_2, \alpha_3]^{\mathsf{T}}$.

6. SPECTRAL UNMIXING OF AN AVIRIS IMAGE

To evaluate the performance of the proposed algorithm for actual data, this section presents the analysis of an hyperspectral image that has received much attention in the remote sensing and image processing communities [13–15]. The image depicted in Fig. 3 has 224 spectral bands, a nominal bandwidth of $10nm$, and was acquired in 1997 by the Airborne Visible Infrared Imaging Spectrometer (AVIRIS) over Moffett Field, at the southern end of the San Francisco Bay, California (see [16] for more details). It consists of a large water point (a part of a lake that appears in dark pixel at the top of the image) and a coastal area composed of vegetation and soil. The data set has been reduced from the original 224 bands to $L = 189$ bands by removing water absorption bands. A 50×50 part of the image represented in gray scale at wavelength $\lambda = 0.66\mu m$ (band 30) has been processed by the proposed unmixing algorithm.

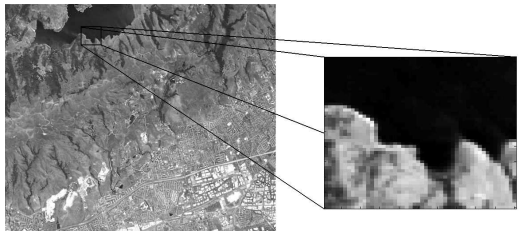

Fig. 3. Real hyperspectral data: Moffett Field acquired by AVIRIS in 1997 (left) and the region of interest at wavelength $\lambda = 0.66\mu m$ shown in gray scale (right).

6.1. Endmember determination

The first step of the analysis identifies the pure materials that are present in the scene. Note that a preliminary knowledge of the ground geology would allow us to use a supervised method for endmember extraction (eg. by averaging the pixel spectra on appropriate regions of interest). Such data being not available, a fully automatic procedure has been implemented. This procedure includes a principal component analysis (PCA) which allows one to reduce the dimensionality of the data and to know the number of endmembers present in the scene as explained in [1]. After computing the cumulative normalized eigenvalues, the data have been projected on the two first principal axes (associated to the two larger eigenvalues). The vertices of the simplex defined by the centered-whitened data in the new 2 dimensional space are determined by the N-FINDR algorithm [7]. The $R = 3$ resulting endmember spectra corresponding to vegetation, water and soil are plotted in Fig. 4 (top).

6.2. Abundance estimation

The Bayesian unmixing algorithm defined in Sections 3 and 4 has been applied on each pixel of the hyperspectral image (using the endmember spectra identified by the PCA step). The image fraction maps for the $R = 3$ pure materials are represented in Fig. 4 (bottom). Note that a white (resp. black) pixel in the map indicates a large (resp. small) value of the abundance coefficient. Note also that the estimates have been obtained by averaging the last $N_r = 800$ simulated samples for each pixel, according to the MMSE principle. The lake area (represented by white pixels in the water fraction map and by black pixels in the other maps) can be clearly recovered.

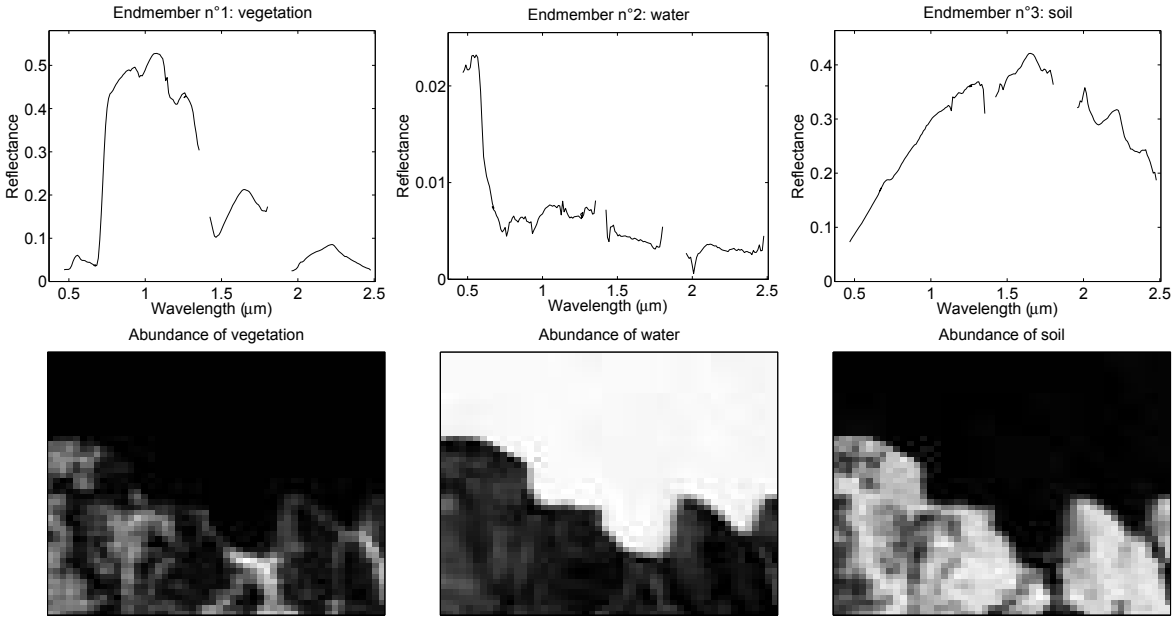

Fig. 4. Top: the $R = 3$ endmember spectra obtained by the N-FINDR algorithm. Bottom: the fraction maps of the corresponding endmember in the scene (black (resp. white) means absence (resp. presence) of the material)

7. CONCLUSIONS

This paper studied a hierarchial Bayesian model for hyperspectral image unmixing. This model provided the posterior distribution of the mixing coefficients (or abundances) which was used for parameter estimation. It is interesting to note that the abundance posterior distribution could also be used to provide information on the significance of the optimally determined parameters such as confidence intervals or theoretical variances. This is the main advantage of the proposed algorithm compared to other approaches. Note also that the algorithm developed in this paper assumed that the number of abundances defining the mixture was known and that the endmembers were belonging to a known dictionary. Future works include the development of Markov chain Monte Carlo methods allowing to remove these hypotheses. A performance comparison between the proposed hierarchical Bayesian methodology and constraint least-squares techniques is also under investigation.

8. ACKNOWLEDGMENTS

The authors would like to thank Prof. Gérard Letac (LSP, Toulouse, France) and Dr. Saïd Moussaoui (IRCCyN, Nantes, France) for their helpful comments on multivariate truncated normal distributions and the Jet Propulsion Laboratory (Pasadena, CA, USA) for freely supplying the AVIRIS data.

9. REFERENCES

[1] N. Keshava and J. F. Mustard, "Spectral unmixing," *IEEE Signal Processing Magazine*, pp. 44–57, Jan. 2002.

[2] C.-I. Chang and B. Ji, "Weighted abundance-constrained linear spectral mixture analysis," *IEEE Trans. Geosci. and Remote Sensing*, vol. 44, no. 2, pp. 378–388, Feb. 2001.

[3] D. C. Heinz and C.-I. Chang, "Fully constrained least-squares linear spectral mixture analysis method for material quantification in hyperspectyral imagery," *IEEE Trans. Geosci. and Remote Sensing*, vol. 29, no. 3, pp. 529–545, March 2001.

[4] D. Manolakis, C. Siracusa, and G. Shaw, "Hyperspectral subpixel target detection using the linear mixing model," *IEEE Trans. Geosci. and Remote Sensing*, vol. 39, no. 7, pp. 1392–1409, July 2001.

[5] J. M. Nascimento and J. M. B. Dias, "Vertex component analysis: A fast algorithm to unmix hyperspectral data," *IEEE Trans. Geosci. and Remote Sensing*, vol. 43, no. 4, pp. 898–910, April 2005.

[6] M. Craig, "Minimum volume transforms for remotely sensed data," *IEEE Trans. Geosci. and Remote Sensing*, pp. 542–552, 1994.

[7] M. Winter, "Fast autonomous spectral end-member determination in hyperspectral data," in *Proc. 13th Int. Conf. on Applied Geologic Remote Sensing*, vol. 2, Vancouver, April 1999, pp. 337–344.

[8] A. Strocker and P. Schaum, "Application of stochastic mixing models to hyperspectral detection problems," in *Proc. SPIE, Algorithms for Multispectral and Hyperspectral Imagery III*, vol. 3071, Orlando, FL, 1997, pp. 47–60.

[9] M. Berman, H. Kiiveri, R. Lagerstrom, A. Ernst, R. Dunne, and J. F. Huntington, "ICE: A statistical approach to identifying endmembers in hyperspectral images," *IEEE Trans. Geosci. and Remote Sensing*, vol. 42, no. 10, pp. 2085–2095, Oct. 2004.

[10] E. Punskaya, C. Andrieu, A. Doucet, and W. Fitzgerald, "Bayesian curve fitting using MCMC with applications to signal segmentation," *IEEE Trans. Signal Processing*, vol. 50, no. 3, pp. 747–758, March 2002.

[11] N. Dobigeon and J.-Y. Tourneret, "Truncated multivariate Gaussian distribution on a simplex," IRIT/ENSEEIHT/TéSA, Tech. Rep., Dec. 2006. [Online]. Available: http://www.enseeiht.fr/~dobigeon

[12] RSI (Research Systems Inc.), *ENVI User's guide Version 4.0*, Boulder, CO 80301 USA, Sept. 2003.

[13] E. Christophe, D. Léger, and C. Mailhes, "Quality criteria benchmark for hyperspectral imagery," *IEEE Trans. Geosci. and Remote Sensing*, vol. 43, no. 9, pp. 2103–2114, Sept. 2005.

[14] F. W. Chen, "Archiving and distribution of 2-D geophysical data using image formats with lossless compression," *IEEE Geosci. and Remote Sensing Letters*, vol. 2, no. 1, pp. 64–68, Jan. 2005.

[15] T. Akgun, Y. Altunbasak, and R. M. Mersereau, "Super-resolution reconstruction of hyperspectral images," *IEEE Trans. Image Processing*, vol. 14, no. 11, pp. 1860–1875, Nov. 2005.

[16] AVIRIS Free Data. (2006) Jet Propulsion Lab. (JPL). California Inst. Technol., Pasadena, CA. [Online]. Available: http://aviris.jpl.nasa.gov/html/aviris.freedata.html